

Huge magneto-crystalline anisotropy of x-ray linear dichroism observed on Co/FeMn bilayers

W. Kuch*

Freie Universität Berlin, Institut für Experimentalphysik, Arnimallee 14, D-14195 Berlin, Germany

F. Offi,[†] L. I. Chelaru,[‡] J. Wang,[§] K. Fukumoto,[¶] M. Kotsugi,^{**} and J. Kirschner
Max-Planck-Institut für Mikrostrukturphysik, Weinberg 2, D-06120 Halle, Germany

J. Kuneš

*Theoretical Physics III, Center for Electronic Correlations and Magnetism,
Institute of Physics, University of Augsburg, D-86135 Augsburg, Germany. and
Institute of Physics, Academy of Sciences of the Czech Republic,
Čukrovarnická 10, 162 53 Praha 6, Czech Republic.*

(Dated: 23.03.2007)

We present an x-ray spectromicroscopic investigation of single-crystalline magnetic FeMn/Co bilayers on Cu(001), using X-ray magnetic circular (XMCD) and linear (XMLD) dichroism at the Co and Fe L_3 absorption edges in combination with photoelectron emission microscopy (PEEM). Using the magnetic coupling between the ferromagnetic Co layer and the antiferromagnetic FeMn layer we are able to produce magnetic domains with two different crystallographic orientations of the magnetic easy axis within the same sample at the same time. We find a huge difference in the XMLD contrast between the two types of magnetic domains, which we discuss in terms of intrinsic magneto-crystalline anisotropy of XMLD of the Co layer. We also demonstrate that due to the high sensitivity of the method, the small number of induced ferromagnetic Fe moments at the FeMn–Co interface is sufficient to obtain magnetic contrast from XMLD in a metallic system.

PACS numbers: 75.70.Ak, 68.37.-d, 75.50.Ee

I. INTRODUCTION

The recent interest in the magnetic coupling between antiferromagnetic (AF) and ferromagnetic (FM) materials is motivated by the quest for fundamental insight into the phenomenon of exchange bias.¹ This effect, the discovery of which dates back to the 1950's,² manifests itself in a shift of the magnetization curve along the field axis. Nowadays the exchange bias effect is employed in a variety of devices, such as sensors or hard disk read heads, based on magnetic thin films.^{3,4}

Only few methods can be used to study the spin structure of ultrathin antiferromagnetic films. While neutron diffraction and Mössbauer spectroscopy have been successfully employed to explore the spin structures of many bulk antiferromagnets already decades ago, both methods suffer from a lack of signal if films of a few atomic layers are to be investigated. X-ray magnetic linear dichroism (XMLD) in the soft x-ray absorption, on the other hand, is a method with sub-monolayer sensitivity. XMLD refers to the difference between x-ray absorption spectra for the plane of x-ray polarization aligned parallel and perpendicular to the atomic moments.⁵ By symmetry the XMLD signal does not depend on the orientation of magnetic moments but only on their axial alignment, and is thus suitable for the investigation of ferromagnetic as well as collinear antiferromagnetic spin structures, antiferromagnetic thin films in particular. Linear dichroism signal is also encountered in case of structural, not magnetic, reduction of the symmetry, as is commonly the

case in the direction along the film normal due to the presence of interfaces.^{6,7} This can be eliminated if measurements are compared in which only the direction of the spin axis is varied, while the lattice geometry is fixed. In the following we will use the acronym “XMLD” for this situation only.

Unlike x-ray magnetic circular dichroism (XMCD), which in 3d metallic systems essentially measures integral quantities, namely the spin and orbital magnetic moments, the size and shape of XMLD depend also on the details of the electronic structure. Although integral sum rules have been put forward for XMLD,⁸ which relate the integral over the XMLD signal to the magneto-crystalline-anisotropy energy, this integral is usually much smaller than the amplitude of the plus-minus feature in the XMLD spectrum. Theoretical calculations predict that the latter may vary significantly with the crystallographic orientation of the magnetic moments.⁹ This is what we call the magneto-crystalline anisotropy of XMLD.

In this paper we study the magneto-crystalline anisotropy of XMLD of a thin Co layer. We use the AF–FM coupling between the FeMn and Co layers to manipulate the orientation of the Co moments, namely the observation that Co moments in a Co/FeMn bilayer align along $\langle 110 \rangle$ directions when in contact with a magnetically disordered (paramagnetic) FeMn layer (above its Néel temperature), while they prefer $\langle 100 \rangle$ directions when the FeMn layer magnetically orders (antiferromagnetic).^{10,11} We take advantage of the fact that the Néel temperature

depends on the thickness of the FeMn layer.¹² Growing wedge-shaped samples we are thus able to study both $\langle 110 \rangle$ - and $\langle 100 \rangle$ -oriented domains at the same time.

We use a photoelectron emission microscope (PEEM), as described in Refs. 13,14,15 for the microscopic laterally resolved detection of the x-ray absorption cross section of the FeMn/Co bilayers. In combination with x-ray magnetic circular dichroism (XMCD) in the soft x-ray absorption as a magnetic contrast mechanism, PEEM is routinely used for the element-resolved observation of magnetic domain patterns in multilayered structures.^{13,16,17} XMLD can equally serve as the magnetic contrast mechanism for PEEM if linearly polarized x-rays are used. Here, a combined XMCD and XMLD spectromicroscopic investigation of single-crystalline FeMn/Co bilayers on Cu(001) is presented. We find that the XMLD signal of the FM Co layer exhibits a strikingly different behavior when in contact with a paramagnetic and an anti-ferromagnetically ordered FeMn layer, while the XMCD contrast does not differ appreciably. We compare our observations to *ab initio* calculations of the L_3 XMLD in bulk fcc Co for different crystallographic orientations of the magnetic moments.

Investigation of the influence of spin and electronic structure on the XMLD requires single-crystalline samples with well characterized AF-FM interfaces. Because of the small lattice mismatch (0.4%),¹⁸ Fe₅₀Mn₅₀ films (FeMn in the following) on a Cu(001) single crystal are ideal candidates for such investigations. Epitaxial, virtually unstrained FeMn films can be grown in a layer-by-layer mode by thermal deposition on Cu(001) at room temperature.¹² This provides an opportunity to study the magnetic properties of an AF/FM system in single crystalline FeMn/Co and Co/FeMn bilayers on Cu(001).^{10,12,19} Scanning tunneling microscopy revealed atomically smooth interfaces with islands or vacancies of single atomic height.²⁰ Based on XMCD-PEEM investigations of FM/FeMn/FM trilayers and on XMLD spectroscopy experiments of Co/FeMn bilayers, we concluded previously that a non-collinear three-dimensional spin structure is present in the ultrathin FeMn layers, possibly similar to the so-called 3Q spin structure present in bulk FeMn.²¹ Combination of the Kerr magnetometry and XMCD-PEEM imaging showed that the magnetic coupling across the interface is mediated by step edges of single atom height, while atomically flat areas do not contribute.²²

II. EXPERIMENT

All experiments were performed *in-situ* in an ultrahigh vacuum system with a base pressure below 10^{-8} Pa. The disk-shaped Cu(001) single crystal was cleaned by cycles of 1 keV argon ion bombardment at 300 K and subsequent annealing at 873 K for 15 minutes. The surface exhibited a sharp (1×1) low energy electron diffraction pattern. No contaminations were detectable by Auger

electron spectroscopy (AES).

The films were grown by thermal evaporation on the clean substrate at room temperature in zero external magnetic field. Fe and Co were evaporated by electron bombardment of high purity wires (99.99% purity) of 2 mm diameter, while a rod (99.5% purity) of 4 mm diameter was used for Mn. Fe_xMn_{1-x} films of equiatomic composition ($x = 0.50 \pm 0.02$) were obtained by simultaneous evaporation of Fe and Mn from two different sources. During the deposition the pressure in the chamber was kept below 5×10^{-8} Pa. A typical evaporation rate was 1 ML per minute. The composition of the FeMn films was estimated from the evaporation rates of the two sources, determined by medium energy electron diffraction (MEED), and cross-checked by Auger electron spectroscopy peak ratios. No indication of segregation of Cu into or on top of the FeMn layers was found. The thickness of the films was determined by MEED, which shows pronounced layer-by-layer oscillations.¹² The FeMn layer was grown in the form of small wedges of 200 μ m width, using the method described in Ref. 23.

The experiments were performed at the UE56/2-PGM1 helical undulator beamline of the Berlin synchrotron radiation facility BESSY, which can be set to deliver circularly polarized radiation of either helicity with a degree of circular polarization of about 80%, or linear vertical or horizontal polarization of $> 97\%$.²⁴ The set-up of the electrostatic PEEM was identical to that described in Refs. 13,14,15. The light was incident at an angle of 30° with respect to the sample surface. Rotation of the sample about the surface normal allowed to take images for different x-ray azimuthal angles of incidence. Parameters were set to a lateral resolution of 350 nm, and a field of view of 60 μ m.

The XMCD images represent a grayscale-coded absorption asymmetry for opposite helicities of the circularly polarized x-rays at the L_3 absorption maximum (777.5 eV),

$$A_{XMCD} = \frac{I_+ - I_-}{I_+ + I_-}, \quad (1)$$

i.e., the difference of absorption images acquired with opposite helicities divided by their sum. For the quantitative analysis, background images acquired at lower photon energy (5 eV below the L_3 maximum) were subtracted.

For XMLD, the maximum contrast was determined from a series of images acquired with 0.2 eV photon energy step around the maximum of the Co L_3 absorption peak of a 6 ML Co/Cu(001) film, using *p*-polarized light. Maximum contrast was found between images taken at photon energies $E_1 = 776.5$ eV and $E_2 = 777.9$ eV. Since the acquisition time necessary to observe XMLD contrast at the Fe L_3 edge in FeMn/Co/Cu(001) bilayers was of the order of hours, no such photon energy sweeps were undertaken for the Fe L_3 edge (maximum at 707.5 eV); instead, the same relative photon energies as determined for the Co L_3 edge were tentatively used ($E_1 = 706.5$ eV

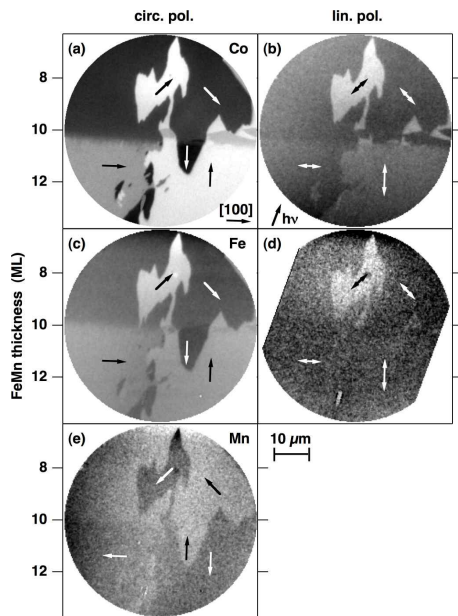


FIG. 1: Magnetic domain images of FeMn/Co/Cu(001) structure obtained at the L_3 edges of (a), (b) Co, (c), (d) Fe, and (e) Mn. The thickness of the FeMn layer, increasing from the top to the bottom of each image, is shown on the vertical axis. Crystallographic orientation of the Cu substrate and azimuthal angle of incidence are shown in panels (a) and (b), respectively. The left and right columns represent the XMCD and XMLD contrast, respectively. Arrows indicate the domain magnetization.

and $E_2 = 707.9$ eV). Images at the two photon energies were taken using s and p polarized x-rays. Because of the 30° incidence, XMLD from in-plane magnetization is larger by a factor of $4/3$ for s polarized excitation. Taking into account the opposite sign of the effect for the two polarizations we used the following formula for the XMLD contrast

$$A_{XMLD} = \frac{1}{2} \left[\frac{I_s(E_2) - I_s(E_1)}{I_s(E_2) + I_s(E_1)} - \frac{4}{3} \frac{I_p(E_2) - I_p(E_1)}{I_p(E_2) + I_p(E_1)} \right]. \quad (2)$$

The images thus reproduce quantitatively the difference between images taken at the higher photon energy minus images taken at the lower photon energy for s polarized x-rays, divided by the sum of these images.

III. RESULTS AND DISCUSSION

This section is divided into three parts. First, we demonstrate the performance of the spectromicroscopic domain imaging and present the contrast obtained on the L_3 edges of Co, Fe and Mn. Next, we study the dependence of the XMCD and XMLD contrast at the Co L_3 edge on the azimuthal angle of incidence. Finally, we discuss the quantitative difference between the XMLD signal obtained from $\langle 110 \rangle$ and $\langle 100 \rangle$ domains.

In Fig. 1 typical XMCD and XMLD images obtained at the L_3 edge of Co are shown together with those obtained at the L_3 edges of Fe and Mn. A wedge-shaped FeMn/12 ML Co bilayer was used. The Co XMCD image (a) shows micron-sized magnetic domains. While the domain magnetization lies along $\langle 110 \rangle$ directions in the upper half of the image, only domains with magnetization along $\langle 100 \rangle$ can be seen in the lower half. This behavior was observed previously,^{10,11} and is related to the fact that for less than about 10 ML FeMn thickness is paramagnetic at room temperature, while thicker FeMn layers develop AF order.¹²

Identical domain patterns with strongly reduced XMCD contrast are observed at the Fe (c) and Mn (e) L_3 edges. The contrast arises due to the induced moments in the FeMn layer.¹⁹ The Mn image is a negative of the Fe and Co images, indicative of an antiparallel orientation of the Mn moments with respect to the magnetization direction of the FM Co layer.

Images of the same spot obtained with XMLD as magnetic contrast mechanism are shown in the right column of Fig. 1. The magnetic domain pattern is clearly visible at the Co L_3 edge (b). Note that domains with opposite magnetization direction cannot be distinguished by XMLD (compare the right lower parts of images (a) and (b)). The XMLD contrast at the Fe L_3 edge is much weaker than at the Co L_3 edge. Only after averaging over images with about 170 minutes total acquisition time we were able to recognize at least the magnetic domains in the top part of the image.

The images of Fig. 1 are presented on quite different grayscale ranges: While the full contrast from saturated white to saturated black in the Co XMCD image (a) is 20%, it is amplified to 8% for the Fe (c) and 1.5% for Mn (e) XMCD images, and amounts to 3% in the Co XMLD image (b), and only 0.7% in the Fe XMLD image (d).

Our previously published XMLD spectra,²¹ in which the XMLD signal at the Fe L_3 edge is below the noise level, supported a non-collinear antiferromagnetic arrangement of Fe spins in the AF FeMn layer. In this case only the small induced ferromagnetic moment in the FeMn layer, the XMCD signal of which corresponds to about 30% of the Fe atoms in the interface atomic layer,¹⁹ leads to an XMLD signal. Although XMLD has been successfully applied in the past to image antiferromagnetic domains in PEEM,^{25,26,27,28} no attempt was made on metallic antiferromagnets, and it is commonly believed that the reduced crystal field splitting of the electronic states in metals^{9,29,30} is prohibiting the use of XMLD for magnetic imaging. Fig. 1 (d), however, shows that it is possible to image the XMLD signal, even of the comparably low number of the induced moments, by PEEM.

Quantitative estimates support the interpretation of the contrast observed in Fig. 1 (d): In the top part of the image, the Fe XMLD is about a factor of 6 weaker than the Co XMLD at the same position. This is about the same ratio as between the respective XMCD contrasts in

panels (a) and (c) at about 6 ML FeMn thickness. This size of induced ferromagnetic alignment is consistent with our earlier investigation of FeMn/Co bilayers.¹⁹ Furthermore, the Fe XMLD originating from induced moments at the interface decreases with increasing total FeMn thickness, so that the expected Fe XMLD signal would be within the noise of the measurement of the spectra of Ref. 21, which were taken for a 15 ML FeMn film.

Fig. 2 shows a series of magnetic domain images of the Co layer from a sample in which a 0–25 ML wedge of FeMn was deposited on top of a continuous film of 6 ML Co/Cu(001). The left column shows the XMCD contrast at the Co L_3 absorption maximum. The right column shows images of the same spot of the sample, acquired with linear polarization of the x-rays. As in Fig. 1, the FeMn thickness increases from the top to the bottom of the images. Panels (a) through (g) show images obtained for different azimuthal angles of incidence, indicated by an arrow at the right hand side of each panel. Note that the field of view slightly shifted due to readjustment of the sample. The azimuth angle was read from a dial at the sample holder with an accuracy of 1° . 0° corresponds to the nominal $[010]$ direction of the Cu substrate; however, as will be outlined below, the angular dependence of the magnetic contrast indicates that the real $[010]$ direction was at -2° azimuth angle. This deviation from the nominal direction is within the accuracy with which the substrate could be oriented upon mounting to the sample holder.

The data have been taken in the sequence from (a) to (g). Typical acquisition times were 4 minutes per helicity for the circular polarization, and 20 minutes per polarization direction and photon energy for the linear polarization. Including the necessary sample manipulations, the time to obtain the data of Fig. 2 totalled 28 hours. The time evolution of the domain pattern is clearly visible in the (a)–(g) series from the shift of the transition line between paramagnetic and antiferromagnetic FeMn towards higher thicknesses. We attribute this to progressing contamination and possibly oxidation by residual gas of the surface of the FeMn layer. The Co layer, however, which is investigated here, is protected against contamination by the FeMn overlayer.

The right column of Fig. 2 shows images taken with linear x-ray polarization. The upper parts of the images clearly reveal identical domain pattern as seen with XMCD. The behavior of the XMLD contrast follows the geometric expectations including the reversal of contrast between panels (a) and (c), and near vanishing of the contrast in panel (b) for the azimuthal angle of incidence close to 45° with respect to the magnetization. The most prominent observation, and the main result of this work, is the strong suppression of the XMLD contrast visible in the bottom parts of the images which correspond to domains with $\langle 100 \rangle$ direction of magnetization.

In the following we discuss the angular dependence of XMCD and XMLD contrast in detail. In Fig. 3 we show the Co XMCD contrast as a function of the azimuthal

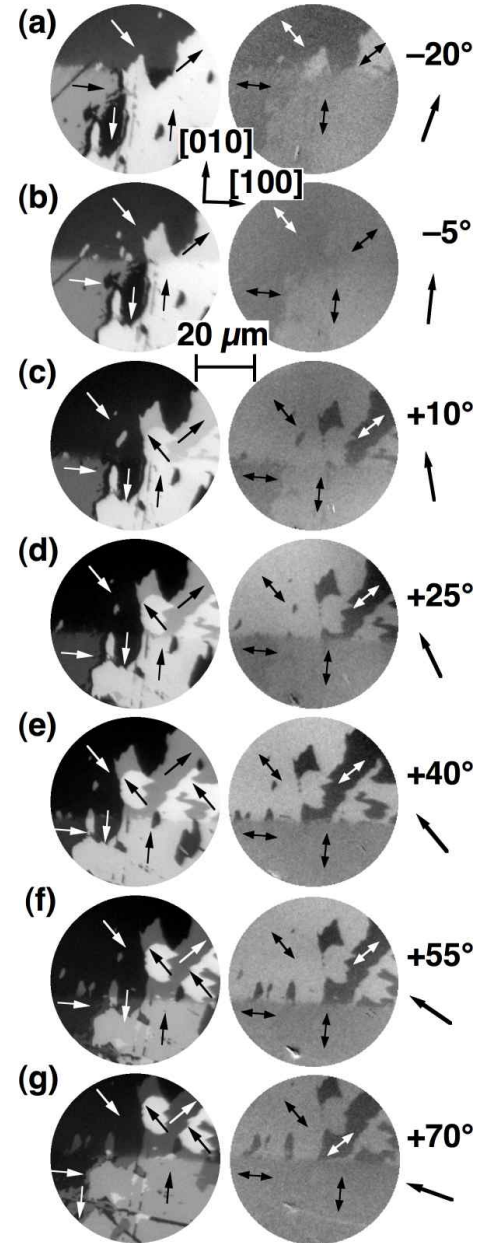


FIG. 2: Magnetic domain images of a FeMn/Co bilayer on Cu(001), acquired at the Co L_3 edge with circular polarization (left column) and linear polarization (right column). Rows (a)–(g) correspond to different azimuthal angles of incidence, as labeled at the right hand side and indicated by arrows. Local magnetization directions are indicated by arrows. The FeMn thickness increases from top to bottom in each image, from 7.2 to 14.7 in (a), gradually shifting to from 9.4 to 16.9 ML in (g).

angle of incidence obtained from the data of Fig. 2. Fig. 3 (a) shows the contrast of the domains in the upper part of the images, where the FeMn is paramagnetic and Co domains are magnetized along $\langle 110 \rangle$ directions. Panel (b) presents the contrast from the lower part of the images, where the FeMn is antiferromagnetic and Co domains

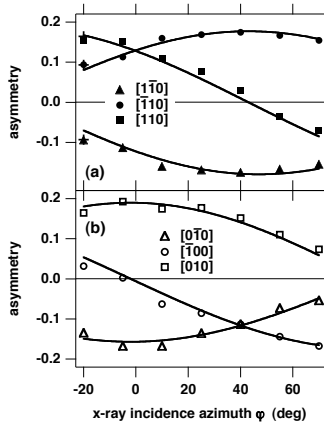


FIG. 3: Angular dependence of the Co L_3 XMCD contrast: (a) the XMCD signal of three domains with magnetization directions $[1\bar{1}0]$, $[\bar{1}10]$, and $[110]$ represented by solid triangles, circles, and squares, respectively (the crosses at -20° are measurements from a Co/Cu(001) reference film without FeMn layer), (b) the XMCD signal of three domains with magnetization directions $[0\bar{1}0]$, $[\bar{1}00]$, and $[010]$ represented by open triangles, circles, and squares, respectively. The solid lines are the result of simultaneous $\sin(\varphi)$ fits to the data.

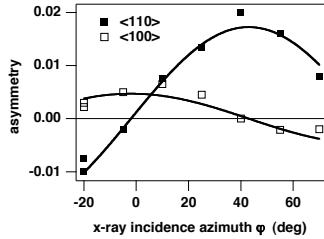


FIG. 4: Angular dependence of the Co L_3 XMLD contrast. The contrast between Co magnetic domains with mutually perpendicular magnetization direction along $\langle 110 \rangle$ directions is represented by solid symbols, the contrast between Co domains with perpendicular magnetization direction along $\langle 100 \rangle$ directions is represented by open symbols. The solid lines are the result of simultaneous $\sin(2\varphi)$ fits to the data.

align along $\langle 100 \rangle$ directions. The lines correspond to a sine fit. The fit reveals a -2° phase shift, which can be attributed to the inaccuracy of the sample mounting. The angular dependence of the XMCD contrast of the individual domains confirms very nicely the assignment of magnetization directions in Fig. 2. A small vertical offset may be attributed to instrumental asymmetries, as for example different intensities of the two helicities. Importantly, the amplitude of the XMCD contrast is only about 5% lower in panel (b) than in panel (a). The latter is equal to the contrast of Co domains in a Co/Cu(001) reference sample without FeMn layer, which is indicated in Fig. 3 (a) by crosses at -20° incidence azimuth.

Fig. 4 shows the angular dependence of the Co XMLD contrast from data of Fig. 2. Solid and open symbols represent the contrast between domains with mutually per-

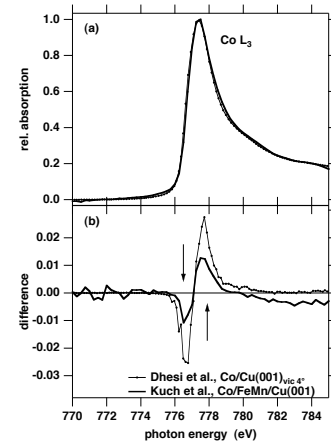


FIG. 5: Comparison of different experimental Co XMLD data from literature. (a): Polarization-averaged absorption at the Co L_3 edge, (b): Difference between absorption for parallel and perpendicular x-ray polarization. Markers and thin lines: Fig. 1 of Ref. 30, for 6 ML Co on 4° miscut Cu(001), magnetization along $\langle 110 \rangle$. Thick lines: Data from Fig. 4 of Ref. 21, for 15 ML FeMn/6 ML Co/Cu(001), magnetization along $\langle 100 \rangle$, scaled to the same absorption maximum. The data of Ref. 30 have been shifted in energy by -1.34 eV for overlap of the absorption curves in (a).

pendicular magnetization direction in the regions where the FeMn layer is paramagnetic and antiferromagnetic, respectively. The solid lines are the result of sine fits for which the phases were fixed at $+43^\circ$ and -2° , respectively, using the result of the fits of Fig. 3. Again, the data confirm the assignment of the magnetization axes in Fig. 2. Based on the fits we are able to quantify the suppression of the XMLD contrast in $\langle 100 \rangle$ domains as compared to the $\langle 110 \rangle$ domains to be a factor of 0.28. Such a large effect of magnetization direction on any physical quantity is rather unusual in 3d metals, which exhibit only a weak spin-orbit coupling. In order to prove that we see a genuine magneto-crystalline anisotropy we next discuss the role of spin non-collinearity and make comparison to other experimental data and theoretical calculations.

Besides changing the easy axis direction in the Co layer, magnetic ordering of the FeMn may also induce a small non-collinearity of the Co moments. Such a non-collinear fanning out of the FM moments in Fe/MnF₂ bilayers as a consequence of the AF-FM coupling was recently suggested on the basis of Mössbauer spectroscopy.³¹ We consider now if a similar scenario can explain our XMLD data. A distribution of the Co spins around a mean direction would lead to a reduction of both the XMCD and XMLD signals compared to the fully aligned case. While the reduction of the XMCD signal is proportional to the reduction of the net moment, XMLD, due to its different angular dependence, is more sensitive and depends also on the distribution of the fanning angles. In the extreme case of moments oriented

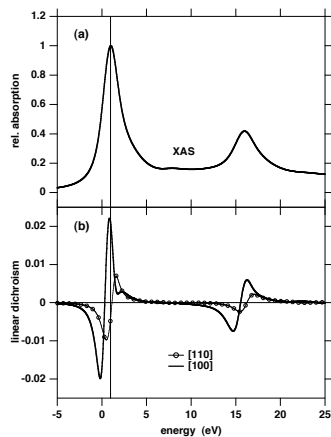


FIG. 6: Calculated XMLD in the fcc Co for magnetization along two different crystallographic directions. (a): Polarization-averaged absorption spectrum for [100] magnetization. (b): XMLD difference for magnetization along [100] (solid line) and along [110] (line and symbols). The data for [100] magnetization are reproduced from Ref. 9. The energy scale is relative to the absorption edge.

at 45° with respect to the net magnetization, the XMLD would be reduced to zero, while the XMCD would still be at 71% of its maximum value. Using the reduction factor of 0.95 of the net magnetization, obtained from XMCD contrast, and assuming both binary (moments point at a fixed angle on either side of the net magnetization) and normal distributions (Gaussian distribution of angles) of the fanning angle we arrive at a reduction factor of about 0.81 for the XMLD contrast. Therefore fanning of the Co moments due to the interaction with the FeMn layer, if at all present, can explain only a small fraction of the observed effect, which amounts to the reduction factor of 0.28.

Since the stability of the instrument is not sufficient to acquire series of microspectroscopic images for different photon energies, we use published data to compare experimental Co XMLD spectra for magnetization along [100] and [110] directions. The [100] data are taken from Ref. 21, in which a 15 ML FeMn/6 ML Co bilayer on Cu(001) was measured. The spectra for Co magnetized along [110] direction are taken from the work of Dhési *et al.*, in which 6 ML Co on Cu(001), miscut by 4° , was measured.³⁰ The two spectra at the Co L_3 edge, rescaled to the same absorption maximum and shifted to the common position of the absorption edge, are compared in Fig. 5. Both spectra had been measured under similar conditions.³² Note that the peak-to-peak ratio of the XMLD spectra of Fig. 5 (b) cannot be compared directly to the ratio of the XMLD asymmetry magnitudes of Fig. 4, which corresponds to the contrast between XMLD signal at the energies marked by arrows in Fig. 5.³³ Although smaller than the asymmetry anisotropy of 3.6 from Fig. 4, the ratio of peak-to-peak XMLD of 2.3 between the two curves obtained from Fig. 5 still indicates substantial magneto-crystalline anisotropy of the XMLD signal.

As mentioned in the Introduction, such a large anisotropy is unusual in 3d metals since the spin-orbit coupling is rather weak, e.g. the calculated magneto-crystalline anisotropy energy in bulk fcc Co is only $2 \mu\text{eV}$ per atom.³⁴ Also the XMCD spectrum, which depends essentially only on integral quantities, namely spin and orbital moments, exhibits a very small anisotropy.⁹ As pointed out by one of us and P. M. Oppeneer, the XMLD signal in metallic Co depends only weakly on the small valence band spin-orbit coupling. The major contribution to XMLD comes from the exchange splitting of the 2p levels ($\approx 1 \text{ eV}$).⁹ The magneto-crystalline anisotropy then arises from the fact that different final 3d states are probed for different orientations of the sample magnetization.

To assess the feasibility of our experimental data, we used the calculated XMLD spectrum of Ref. 9 for the [100] direction (what is referred to in Ref. 9 as “full calculation”) and augmented these with equal calculations for the [110] magnetization on the same system (see Fig. 6). In the calculations performed on bulk fcc Co a sizable anisotropy of XMLD is found, however, the [100] exhibits larger XMLD magnitude contrary to the experiment. Before dismissing these results as a disagreement a few remarks are in order. First, the calculations were done on bulk material while the experiment is performed on a thin layer sandwiched by other materials, therefore a good quantitative agreement is unlikely. Second, we cannot judge the calculated anisotropy based on the present data only. Note that due to a slight mutual shift of the calculated spectra, the [100] contrast at the maximum amplitude of the [110] XMLD would be rather small. Such a shift is not present in Fig. 5, where [100] and [110] spectra obtained on slightly different samples are compared. Third, a possible non-collinearity of Co spins due to the presence of the AF FeMn layer would lead to local moments pointing neither along [110] nor fully along [100]. Taking these uncertainties into account we draw a modest, nevertheless non-trivial, conclusion that the theory does not prohibit a magneto-crystalline anisotropy of XMLD as large as observed in our experiment.

IV. CONCLUSIONS

We have presented a spectromicroscopic PEEM investigation of the magnetic domain pattern on Co/FeMn bilayers using XMCD and XMLD as the contrast mechanism. The sensitivity of the method allows to visualize even the tiny XMLD signal of the induced ferromagnetic moments in the FeMn layer. We have found a factor of 3.6 difference in the XMLD contrast between the Co L_3 signal from $\langle 110 \rangle$ and $\langle 100 \rangle$ domains in a *single* sample. We argue that this huge difference is mainly due to an intrinsic magneto-crystalline anisotropy of XMLD of the Co layer. Comparison of experimental XMLD spectra obtained from different samples published previously and *ab initio* calculations on bulk fcc Co suggest that

such an anisotropy is indeed possible.

Acknowledgments

We thank B. Zada and W. Mahler for technical assistance, and S. S. Dhesi for providing the data from Ref. 30.

-
- * Electronic address: kuch@physik.fu-berlin.de; URL: <http://www.physik.fu-berlin.de/~ag-kuch>
- † Present address: CNISM and Dipartimento di Fisica, Università Roma Tre, Via della Vasca Navale 84, I-00146 Roma, Italy.
- ‡ Present address: Universität Duisburg–Essen, Institut für Experimentelle Physik, Lotharstraße 1, D-47057 Duisburg, Germany.
- § Present address: Department of Physics and HKU-CAS Joint Lab on New Materials, The University of Hong Kong, Hong Kong, China.
- ¶ Present address: SPring-8, 1–1–1 Kouto, Sayo-cho, Sayo-gun, Hyogo 679-5198, Japan.
- ** Present address: Hiroshima Synchrotron Radiation Center, 2–313 Kagamiyama, Higashi-Hiroshima, 739-8526 Hiroshima, Japan.
- ¹ J. Nogués and I. K. Schuller, *J. Magn. Magn. Mater.* **192**, 203 (1999).
 - ² W. H. Meiklejohn and C. P. Bean, *Phys. Rev.* **102**, 1413 (1956).
 - ³ B. Dieny, V. S. Speriosu, S. S. P. Parkin, B. A. Gurney, D. R. Wilhoit, and D. Mauri, *Phys. Rev. B* **43**, 1297 (1991).
 - ⁴ J. C. S. Kools, *IEEE Trans. Magn.* **32**, 3165 (1996).
 - ⁵ G. van der Laan, B. T. Thole, G. A. Sawatzky, J. B. Goedkoop, J. C. Fuggle, J.-M. Esteve, R. Karnatak, J. P. Remeika, and H. A. Dabkowska, *Phys. Rev. B* **34**, 6529 (1986).
 - ⁶ M. W. Haverkort, S. I. Csiszar, Z. Hu, S. Altieri, A. Tanaka, H. H. Hsieh, H.-J. Lin, C. T. Chen, T. Hibma, and L. H. Tjeng, *Phys. Rev. B* **69**, 020408(R) (2004).
 - ⁷ E. Arenholz, G. van der Laan, R. V. Chopdekar, and Y. Suzuki, *Phys. Rev. B* **74**, 094407 (2006).
 - ⁸ G. van der Laan, *Phys. Rev. Lett.* **82**, 640 (1999).
 - ⁹ J. Kuneš and P. M. Oppeneer, *Phys. Rev. B* **67**, 024431 (2003).
 - ¹⁰ W. Kuch, F. Offi, L. I. Chelaru, M. Kotsugi, K. Fukumoto, and J. Kirschner, *Phys. Rev. B* **65**, 140408(R) (2002).
 - ¹¹ C. Won, Y. Z. Wu, H. W. Zhao, A. Scholl, A. Doran, W. Kim, T. L. Owens, X. F. Jin, and Z. Q. Qiu, *Phys. Rev. B* **71**, 024406 (2005).
 - ¹² F. Offi, W. Kuch, and J. Kirschner, *Phys. Rev. B* **66**, 064419 (2002).
 - ¹³ W. Kuch, R. Frömter, J. Gilles, D. Hartmann, C. Zietzen, C. M. Schneider, G. Schönhense, W. Swiech, and J. Kirschner, *Surf. Rev. Lett.* **5**, 1241 (1998).
 - ¹⁴ W. Kuch, L. I. Chelaru, F. Offi, M. Kotsugi, and J. Kirschner, *J. Vac. Sci. Technol. B* **20**, 2543 (2002).
 - ¹⁵ M. Kotsugi, W. Kuch, F. Offi, L. I. Chelaru, and J. Kirschner, *Rev. Sci. Instrum.* **74**, 2754 (2003).
 - ¹⁶ J. Stöhr, Y. Wu, B. D. Hermsmeier, M. G. Samant, G. R. Harp, S. Koranda, D. Dunham, and B. P. Tonner, *Science* **259**, 658 (1993).
 - ¹⁷ W. Kuch, *Appl. Phys. A* **76**, 665 (2003).
 - ¹⁸ Y. Endoh and Y. Ishikawa, *J. Phys. Soc. Jpn.* **30**, 1614 (1971).
 - ¹⁹ F. Offi, W. Kuch, L. I. Chelaru, K. Fukumoto, M. Kotsugi, and J. Kirschner, *Phys. Rev. B* **67**, 094419 (2003).
 - ²⁰ W. Kuch, L. I. Chelaru, and J. Kirschner, *Surf. Sci.* **566–568**, 221 (2004).
 - ²¹ W. Kuch, L. I. Chelaru, F. Offi, J. Wang, M. Kotsugi, and J. Kirschner, *Phys. Rev. Lett.* **92**, 017201 (2004).
 - ²² W. Kuch, L. I. Chelaru, F. Offi, J. Wang, M. Kotsugi, and J. Kirschner, *Nature Mater.* **5**, 128 (2006).
 - ²³ W. Kuch, J. Gilles, F. Offi, S. S. Kang, S. Imada, S. Suga, and J. Kirschner, *J. Electron Spectrosc. Relat. Phenom.* **109**, 249 (2000).
 - ²⁴ M. R. Weiss, R. Follath, K. J. S. Sawhney, F. Senf, J. Bahrtdt, W. Frentrop, A. Gaupp, S. Sasaki, M. Scheer, H.-C. Mertins, et al., *Nucl. Instr. and Meth. A* **467–468**, 449 (2001).
 - ²⁵ J. Stöhr, A. Scholl, T. J. Regan, S. Anders, J. Lüning, M. R. Scheinfein, H. A. Padmore, and R. L. White, *Phys. Rev. Lett.* **83**, 1862 (1999).
 - ²⁶ A. Scholl, J. Stöhr, J. Lüning, J. W. Seo, J. Fompeyrine, H. Siegwart, J.-P. Locquet, F. Nolting, S. Anders, E. E. Fullerton, et al., *Science* **287**, 1014 (2000).
 - ²⁷ F. Nolting, A. Scholl, J. Stöhr, J. W. Seo, J. Fompeyrine, H. Siegwart, J.-P. Locquet, S. Anders, J. Lüning, E. E. Fullerton, et al., *Nature* **405**, 767 (2000).
 - ²⁸ H. Ohldag, A. Scholl, F. Nolting, S. Anders, F. U. Hillebrecht, and J. Stöhr, *Phys. Rev. Lett.* **86**, 2878 (2001).
 - ²⁹ M. M. Schwickert, G. Y. Guo, M. A. Tomaz, W. L. O'Brien, and G. R. Harp, *Phys. Rev. B* **58**, R4289 (1998).
 - ³⁰ S. S. Dhesi, G. van der Laan, and E. Dudzik, *Appl. Phys. Lett.* **80**, 1613 (2002).
 - ³¹ W. A. A. Macedo, B. Sahoo, V. Kuncser, J. Eisenmenger, I. Felner, J. Nogués, K. Liu, W. Keune, and I. K. Schuller, *Phys. Rev. B* **70**, 224414 (2004).
 - ³² Normal incidence, room temperature, degree of linear polarization 95% (Ref. 30), > 97% (Ref. 21), photon energy resolution 400 meV (Ref. 30), 300 meV (Ref. 21), measured under 7 T magnetic field (Ref. 30) and in remanence (Ref. 21).
 - ³³ The left axis of Fig. 4 gives the difference of the raw XMLD asymmetry between the two orthogonal domains. To compare to the spectra of Figs. 6 and 5, one has to keep in mind that the intensity at these two photon energies, in particular the one 1.0 eV below the L_3 peak maximum, is less than the intensity in the peak maximum. In the case of Co the average intensity of the denominator of the asymmetry is about 75% of the peak maximum. Because the difference was normalized to the sum, this has to be doubled and gives a factor of 1.5. The pre-edge background, which is included here, has also to be taken into account. From im-

ages acquired in the Co pre-edge region it was determined to make up for about 35% of the intensity measured at the L_3 maximum. This leads roughly to another factor of 1.7. An asymmetry value of 0.017 in Fig. 4 (the amplitude of the fit curve for $\langle 110 \rangle$ magnetization) thus corresponds to a peak-to-peak amplitude of the linear dichroism of about

4.3% of the L_3 peak height. The curve of Dhesi *et al.*, for comparison, shows a peak-to-peak dichroism of 5.3% of the L_3 peak height.

³⁴ J. Trygg, B. Johansson, O. Eriksson, and J. M. Wills, Phys. Rev. Lett. **75**, 2871 (1995).